Site effects in the Pollino region from the HVSR and polarization of seismic noise and earthquakes

Ferdinando Napolitano[(1)], Anna Gervasi[(3)], Mario La Rocca[(2)], Ignazio Guerra[(2)], Roberto Scarpa[(1)]

(1) Università di Salerno;

(2) Università della Calabria;[1]

(3) Istituto Nazionale di Geofisica e Vulcanologia.

Abstract

Site effects have been studied at 15 sites in the area of Mt Pollino (Italy) through the analysis of seismic noise and earthquakes by horizontal-to-vertical spectral ratios (hereafter referred as HVSR) and polarization methods. The spectral ratio HVSR method has been applied to seismic noise and to 83 local and regional earthquakes with the aim to investigate site effects in the 0.5 – 20 Hz frequency band. At least 20 hours of seismic noise were selected at each site by taking into account day and night hours, and week days during several months in order to include any possible environmental condition. Results show stable HVSR curves characterized by small standard deviation, without high peaks at most stations. The same method was also applied to S waves and early coda waves of earthquakes, showing for most of the sites results very similar to the HVSR curve obtained from the seismic noise. At some sites the HVSR is very flat, with amplitude levels between 0.7 and 2 in the entire considered frequency band. Some other sites show well defined peaks of amplitude up to 4.5. The relationship of site effects seen in the HVSR curves with the local structure have been further investigated through polarization analysis of seismic noise. Results indicate that topography gives the main contribution to site effects in four

[1] Anna Gervasi works also at (2) Università della Calabria (Double affiliation)

cases, while the effects possibly associated with fault zones nearby some stations are less obvious.

Introduction

Site effects can strongly affect seismic wave propagation, modifying duration, amplitude, frequency content and causing polarization of ground motion. Such effects are produced by the local geological structure, as in the case of sedimentary basin where the strong impedance contrast between sediments and the underlying bedrock causes resonance and subsequent amplification of waves which interfer constructively (Pitilakis K., 2004; Panzera et al., 2015). Soft soils amplify the ground motion respect to more compact underlying soils or bedrock. The site amplification depends on the frequency of ground motion and on the impedance contrast between soil and bedrock (Aki, 1993). Amplification of ground motion upon soft soils compared with the shaking observed at nearby bedrock sites have been observed in a great number of earthquakes during the last decades (Singh and Ordaz, 1993; Lachet et al., 1996; Bonilla et al., 1997; Parolai et al., 2010; Clemente-Chavez et al., 2014). This effect can increase significantly the damage produced by earthquakes, even in cases of moderate magnitude events (Castro et al., 2004; Strollo et al., 2007; Cantore et al., 2011; Gallipoli et al., 2013; Nunziata et al., 2014; Cultrera et al., 2016), therefore understanding and predicting ground amplification produced by the interaction of seismic waves with the local geological structure is crucial.

The basic technique to estimate the site response is the earthquake spectral ratio method (Standard Spectral Ratio, SSR, Borcherdt, 1970; Borcherdt and Gibbs, 1976), which is based on the ratio between the spectrum at a site of interest and the spectrum at a reference site computed for the same earthquake. Usually the reference site is a nearby rock site that is assumed not to be affected by site amplification. Common applications of the method imply the SSR calculation on

coda waves (Phillips and Aki, 1986; Chin and Aki, 1991; Mayeda et al., 1991; Koyanagi et al., 1992; Kato et al., 1995; Su and Aki, 1995) as well as on direct S-waves (Lermo et al. 1993; Steidl, 1993; Margheriti et al., 1994; Kato et al., 1995; Hartzell et al., 1996). Also ambient noise signals can be affected by site effects, providing prediction of the site response through empirical techniques such as the horizontal-to-vertical spectral ratio (HVSR). In this case the spectral ratio is calculated by using the vertical component instead of the reference station. For this reason the H/V spectral ratio (HVSR) of background seismic noise, also called "Nakamura method" (Nakamura, 1989), is probably the most used technique for the study of site effects. This method, first introduced by Nogoshi and Igarashi (1970) based on the previous studies of Kanai and Tanaka (1961), revealed very efficient to estimate the site response in case of simple layered structures. However, in case of complex geological structures the interpretation of results is less obvious.

Site effects can also produce the so called "directional site resonance" (Bonamassa and Vidale, 1991), which occur when the horizontal ground motion is amplified in a site-specific azimuth more than other directions. This kind of site effect is observed as ground motion polarized along a site-specific direction. Two important causes have been recognized to produce such effects: fault damage zones (Pischiutta et al., 2012, 2014, 2015, 2017; Panzera et al., 2015, 2017a, 2017b), and topographic irregularities (Chávez-Garcìa et al., 1997; Rigano et al., 2008; Buech et al., 2010; Pischiutta et al., 2010; Formisano et al., 2012). Fault zones often correspond to quite complex geological structures, thus the combination of several phenomena of wave propagation (reflection, resonance, wave trapping) modifies in different amount the amplitude of horizontal motion components, resulting in a polarization nearly parallel (trapped Love waves) to the fault strike. The interaction of seismic waves with the topography also changes the relative amplitude of horizontal motion parallel and normal to the local slope or to the ridge. Topography effects usually manifest as a horizontal polarization nearly orthogonal to the ridge elongation. For

these reasons the joint observation of HVSR and polarization analysis may give a more exhaustive interpretation of site effects.

The aim of this paper is the evaluation of site effects in the Mt. Pollino area (Southern Italy) using HVSR method applied to both seismic noise and earthquakes, and taking further insight from the results of polarization analysis. The Pollino Massif (Figure 1) is a short and stocky mountain range EW oriented, perpendicular to the local axis of the Italian peninsula. Its eastern end rises from the Ionian Sea, while the western one is marked by the steep valley of the Lao River that springs out from the northern slope of the range, near Viggianello, with the name of Mercure and gives its name to the E-W oriented valley at the northern feet of the massif. In correspondence of the village of Laino Borgo, the river changes both name and orientation, turning SW towards the Tyrrhenian Sea. The chain reaches its maximum elevation with the 2267 m of Serra Dolcedorme. From the geological point of view the Pollino area is located at the junction between the southern Apennines northeast-verging collision orogen and the Calabrian rollback subduction zone. Until a couple of decades ago it was generally considered as a gap of the seismicity along the Italian backbone due to the lack of strong local earthquakes in historical times. Recent seismic catalogs and papers include maximum magnitudes in the 5.2 – 6.0 range (e.g., 1693 and 1708 earthquakes; Rovida et al., 2011; Tertulliani and Cucci, 2014). Moreover, paleoseismological investigations of the southern slope of the Pollino area have identified at least two surface-rupturing seismic events between the sixth and fifteenth centuries A.D. corresponding to earthquakes of magnitude 6.5 – 7 (Cinti et al., 2002), leading to values of the seismic hazard official maps increased respect to the preceding ones (Gruppo di Lavoro MPS, 2004). Sound evidence exists (Gervasi et al., 2012; Guerra et al., 1974) of sporadic near-surface microseismic sequences which affected in the past centuries the villages of Mormanno and Morano, near the western edge of the ridge. Moreover, even in absence of written documentation, the occurrence of frequent microearthquakes is well alive in the memory of the Mormanno

inhabitants. The last of these sequences started in the summer 2010 and lasted until the end of 2013. It was different from the preceding ones due to its unusual duration and maximum energy. Earthquake hypocentres were distributed in two dense groups (Figure 2) around two mainshocks of ML4.3 and ML5.1 (Totaro et al. 2013, 2015; Passarelli et al., 2015; Cheloni et al., 2017). We have performed a detailed study of the site response in the area in order to integrate seismic hazard assessments. We have used both seismograms acquired during the above mentioned seismic sequence as well as newly acquired recordings of regional and local earthquakes.

Analysis methods

The HVSR method consists of computing the horizontal-to-vertical spectral ratio of seismic signals. The basic assumption of the HVSR method is that the vertical component of the ground motion is supposed to be free of any kind of influence related with the soil conditions at the recording site in cases where the soil stratigraphy is flat and horizontal. In such cases the HVSR is expected to be characterized by one or more peaks at frequencies corresponding to the soft layers thickness. Moreover, the peak amplitude should be related to the impedance contrast between soft soil and bedrock. Some authors found that HVSR computed for earthquake signals provides a reliable estimate of the site response (Lachet et al., 1996), but the same technique in some cases underestimates the local amplification if compared with that inferred by a reference site method (Borcherdt, 1970). However, due to its low cost and easy applicability, the HVSR method applied to microtremors (Nakamura, 1989) has been extensively used in the last decade, often for microzonation purposes (Strollo et al., 2007).

HVSR method applied to seismic noise

We first applied the HVSR method to seismic noise. At least 20 hours (up to 37 hours in one case) of noise recordings were selected for each site (Figure 1), chosen at different time during night and day, for different week days during several months. Since some of the used stations were installed at short distance from houses and roads, we excluded from the analysis those data affected by transient signals like passage of vehicles and similar disturbances. Recordings which contained earthquakes were excluded as well from this analysis. The spectral analysis was computed on 20 s sliding window, then the average HVSR and its standard deviation were estimated and results are shown in Figure 3. The adopted noise selection criteria revealed to be fairly robust, as confirmed by the stability of results and by the small values of standard deviation, thus we are confident that observed HVSR are reliable and representative of each studied site. We restricted the observation of HVSR results to the 0.5 – 20 Hz frequency band because this is more than enough for engineering purposes in the investigated area, and because in that frequency band we expect the main contribution from the local geological structures. The H/V spectral ratio of seismic noise was also computed as a function of frequency and azimuth to investigate the directional properties of the seismic wavefield.

HVSR method applied to earthquakes

The HVSR analysis was applied to 83 local and regional earthquakes (Table 1 and Table 2). Figure 2 shows the epicenters of all earthquakes located in the area between 2010 and 2014, some of the events analyzed in this paper (red circles), and the two mainshocks (orange stars). Regional earthquakes were selected by requiring the SNR greater than 3 in the frequency band 0.5 – 10 Hz. Thousands of local earthquakes were recorded at some stations, so we could choose events with high SNR in the entire 0.5 – 20 Hz frequency band considered in this work. Signal spectra, and hence the HVSR, were computed on 20 s windows containing the direct S wave and

early coda for regional earthquakes, while 10 s window length was used for local events. For any earthquakes the HVSR was computed also on the seismic noise preceding the event and compared with the average noise result in order to verify the stability of seismic noise features. Some of the seismic stations used in this work were installed during the seismic sequence to better follow its evolution, therefore they were not operating at the same time. For this reason only a few earthquakes with high SNR were recorded at some sites. We analyzed 83 earthquakes recorded at 15 sites, as resumed in Table 1 and Table 2, for a total amount of 276 HVSR curves as shown in Figure 4.

Polarization analysis of seismic noise

The presence of directional effects in the ground motion has been estimated through a polarization analysis of noise recordings computed in time domain (Montalbetti and Kanasewich, 1970). The polarization angle in the horizontal plane has been calculated from the eigenvalues and eigenvectors of the covariance matrix of three-component data, defined by:

$$S_{ij} = \frac{1}{N}\sum_{k=1}^{N} A_i^k A_j^k$$

where A^k_j is the k-th sample of the j-th component of ground motion (j = Z, NS, EW). The polarization direction of the particle motion is given by the eigenvector of the covariance matrix associated with the largest eigenvalue. The "polarization azimuth" is defined as the angle between the North and the projection of the polarization vector on the horizontal plane. Results of this analysis are plotted in polar histograms with azimuth shown in intervals of ten degrees. Polarization analysis of the seismic noise used to estimate the HVSR was computed to see if the polarization direction is frequency dependent. The length of the moving window was chosen in

order to contain at least two periods at the frequency corresponding to the center of the bandpass. Polarization analysis in time domain gives a very clear picture of the signal polarization in the horizontal plane, but does not account for the H/V amplification. Therefore we also computed the HVSR as a function of the azimuth by using the software GEOPSY. The result of such analysis shows by a color scale the H/V ratio as a function of both frequency and azimuth, thus giving an important indication of the frequency band within which the wavefield is polarized.

Results

The results obtained from the HVSR analysis of seismic noise are shown in Figure 3, where the average HVSR curve with its standard deviation is plotted for each investigated site. Results show some features common at groups of sites and some features which characterize individual sites, as described below.

- MMN1, MMN3, MMN4, MMN7, MMNB, T0711, T0713, T0714, T0716 are sites characterized by HVSR of amplitude almost always lower than 2. A few peaks of amplitude between 2 and 3 are present at some of these stations. Seven of these nine sites are characterized by competent rocks (limestone) at surface or very near to the surface, while MMN4 is located upon highly fractured limestone and T0716 is located upon thick recent deposits (Figure 1).
- At MMN and MMN5 the HVSR is higher than 2 for any frequency greater than 3 Hz in the considered band. Two peaks of amplitude 4 at 7 Hz and 16 Hz are seen at MMN, while a broad peak of amplitude greater than 5 at frequency of 10 Hz characterizes MMN5. These results indicate that the two sites are affected by a relevant amplification in spite of the competent local lithology.

- At MMN2 the HVSR curve is greater than 2 in the frequency range 4-11 Hz, with a sharp peak of amplitude 3.5 around 5.5 Hz and two peaks of amplitude 3 at 9.5 Hz and 10.5 Hz. The high peaks at this site were unexpected considering the competent local lithology.
- MMN6, located upon competent rock (limestone), shows large HVSR values (greater than 2) in the frequency range 1-10 Hz, with two separate stable peaks of amplitude 4 around 2.8 Hz and 4.3 Hz.
- MMN7 is characterized by nearly flat HVSR, with a broad peak of amplitude greater than 2 in the frequency range 2-4 Hz. This site is characterized by quite competent lithology.
- T0711 is a site characterized by competent lithology and its HVSR shows amplitude around 2 in the frequency range between 3-12 Hz.
- At T0713 the HVSR curve is nearly flat in the entire considered frequency band, but it shows the highest standard deviation among the analyzed sites, particularly between 1 Hz and 8 Hz. The shallow lithology consist of compact limestone.
- MMN9 shows values of HVSR greater than 2 in the frequency range 1-9 Hz and two sharp peaks around 8 Hz and 11 Hz. The peak at 8 Hz has amplitude of 4.5, the highest and better defined among those observed in this study. The observed HVSR is compatible with the local geology characterized by consolidated deposits of unknown thickness.
- At MMNA and T0711 the HVSR curves are characterized by values around 2 in a wide frequency band between 2 Hz and 12 hz, but without any clear peaks. MMNA station was installed upon schists of poor competence, while T0711 site is characterized by quite competent dolostones.

Results of noise analysis suggest that many sites are characterized by negligible site effects

(MMN1, MMN3, MMN7, MMNB, T0711, T0713, T0714). This result agree very well with the geological features of those sites, which are characterized by bedrock or quite competent rock outcropping or at very shallow depth. The sites MMN4 and T0716 are also characterized by small or negligible amplification, even though the local geology consists of low competent formations. The sites where the HVSR curve indicates likely significant site effects are MMN, MMN2, MMN5, MMN6, MMN9. These five sites show at least one peak of amplitude greater than 3 at frequency lower than 10 Hz, that likely indicates the resonance of the local structure. Since MMN and MMN2 are sites inside the village of Mormanno, their HVSR result is of particular interest for engineering and risk reduction purposes. It is noteworthy that all the five sites characterized by significant amplification are located upon competent lithology. This feature suggests that the cause of amplification must be independent from the local geological structure.

The most of results are characterized by small standard deviation (less than 0.3) in the entire considered frequency range, with many values smaller than 0.1. Only in a few cases, like T0713, the standard deviation is greater than 0.5 in some frequency ranges. The low values of standard deviation, associated with the large amount of analyzed noise (at least 20 hours for each site), indicate that the observed HVSR curves are reliable and possibly representative of site response.

Results obtained from the analysis of 83 earthquakes selected at the 15 sites are shown in Figure 4 by 276 HVSR curves. Each plot of this Figure shows curves of individual analyzed earthquakes and the average among them by blue line. The number of analyzed earthquakes is different for each site, from a minimum of 7 to a maximum of 52, depending on the data available at the corresponding seismic station. The comparison between HVSR computed for earthquakes and the average HVSR of seismic noise is shown in Figures 5, 6, and 7. For the most of analyzed sites the results of earthquakes are very similar in shape and amplitude with the HVSR of

background noise. The main features of these results are described below.

- MMN1, MMN3, MMNB, T0714, T0716 show a nearly flat HVSR that suggest the absence of strong resonance associated with the local geological structure (Figures 5 and 7). At these sites the HVSR are very similar to those of seismic noise and take the most of their values between 1 and 2. Only T0716 among these five sites is characterized by low competent lithology.

- At MMN the HVSR are different from any other sites, with the highest amplitude at frequency greater than 12 Hz (Figures 4 and 5). This trend is similar to the result found from noise, but without the sharp peak at 7 Hz (Figure 5).

- At MMN2 the earthquake HVSR are quite different than the results found from the analysis of seismic noise, particularly at frequency lower than 11 Hz. The peak at 5.5 Hz and the two peaks at 9.5 Hz and 10.5 Hz that characterize the noise are not present in the earthquake HVSR (Figure 5). This difference suggests that the peaks seen in the noise results are not produced by a resonance of the local structure, which consists of competent lithology, but more likely by topography effects, being this site located on the edge of a small ridge. This hypothesis is also supported by the results of polarization analysis, as described below.

- At MMN4 and MMN7 the HVSR are nearly flat for frequency greater than 4 Hz, but show a peak of low amplitude (about 3) at frequency around 1 - 2 Hz. This feature is only partially seen in the noise HVSR at MMN7, while there is no correspondence at MMN4 (Figure 6).

- At MMN5 the HVSR shows the highest peaks among the 15 sites, with some higher than 5 at frequency greater than 8 Hz. Earthquakes and noise show fairly similar results.

- At MMN6 the HVSR have a trend very similar to that observed from the seismic noise, characterized by a high peak at low frequency (1-3 Hz) and regular decreasing amplitude up to 12 Hz. However, the two noise peaks around 2.8 Hz and 4.3 Hz are not clearly separated in the earthquake HVSR.
- Regarding the comparison between earthquake and noise results, significant differences are observed only at four sites: MMN, MMN2, MMN5, T0713.

The direction of particle motion in the horizontal plane have been evaluated through the polarization analysis of seismic noise performed on signals bandpass filtered in the four frequency bands 1 – 2 Hz, 2 - 4 Hz, 3 - 5 Hz and 4 - 8 Hz. Results are shown in Figures 8 and 9. For any stations polar histograms are shown by different colors for two different frequency bands. Each histogram represents the stacking of all the seismic noise recorded at that station. Among the 15 studied sites only MMNA and T0714 show a polarization distribution roughly isotropic at any frequencies. A roughly isotropic polarization is seen only at low frequency (1 – 2 Hz, blue in Figure 8) also at stations MMN4, MMN5, MMN7, MMN9. All other sites are characterized by a well defined direction of the horizontal particle motion. These features are very similar in each of the three higher frequency bands, as shown in Figures 8 and 9. However, the polarization azimuth may vary strongly with frequency, and above all, the H/V ratio depends from both frequency and azimuth. This is seen in Figure 10, where the H/V ratio is shown for each site as a function of frequency and azimuth. Figure 10 shows clearly as the two sites MMN and MMN5 are characterized by high values of H/V ratio strongly dependent from frequency and azimuth, as expected from the polarization histograms shown in Figures 8 and 9, and from the HVSR shown in Figure 3. The main peaks that characterize the HVSR at MMN6 (3 Hz and 5 Hz) and MMN9 (8 Hz and 11 Hz) are also well polarized. Since the directions of polarization are very different

from each site to the others, even at distance as short as few hundreds meters (MMN, MMN1, MMN2, MMN3, MMN5, see Figure 1), it may not be a feature of the background noise, but it is likely a site effect. Polarization of the particle motion of seismic noise is known to be modified by topography (Chávez-Garcìa et al., 1997; Rigano et al., 2008; Buech et al., 2010; Pischiutta et al., 2010; Formisano et al., 2012) and heterogeneities in the local structure, such as fault zones (Pischiutta et al., 2012, 2014, 2015, 2017; Panzera et al., 2015, 2017a, 2017b).

Discussion and conclusions

The analysis of site effects carried out by computing the HVSR curves on the background seismic noise at 15 sites has been enriched by the same analysis performed on local and regional earthquakes, and furthermore by the polarization analysis. The comparison of HVSR curves obtained from noise and from earthquakes shows that they are quite similar in the most of analyzed sites. However, in four cases of the 15 analyzed sites some significant differences are observed (MMN, MMN2, MMN5, T0713). To explain those differences we look at the results of polarization analysis and try to correlate them with topography and other geological irregularities. The relationship between polarization direction and local slope has been estimated qualitatively and results are resumed in Table 3. At nine sites the polarization direction is very similar or equal to the slope direction, while at only three sites it is roughly normal to the slope direction. The last two sites do not show a well defined polarization direction. To investigate any possible relationship between polarization and other geological structures we took into account the known faults near the analyzed sites, as shown in Figure 1. Results of the angle between the polarization direction and fault strike, and the approximate distance to the fault, are resumed in Table 4. For this qualitative analysis we considered only those known faults that are closer than 250 m from the analyzed sites, therefore only 5 sites are taken into account. At three of these 5 sites the

polarization direction is roughly normal to the fault strike, as observed by some authors in other regions (Rigano et al., 2008; Pischiutta et al., 2012, 2014, 2015, 2017), while the other two sites show polarization oblique to the fault strike. We do not observe any polarization parallel to the fault strike, which would suggest the presence of trapped waves in the fault zone. Therefore no clear effects in the seismic wavefield can be ascribed to near faults at the analyzed site. On the other hand, this is not surprising because the considered faults are minor faults without a well developed fault zone. Now we can reconsider the four sites where the HVSR from noise and earthquakes are significantly different (MMN, MMN2, MMN5, T0713). At all of them the polarization direction is parallel to the slope direction that characterize the topography. In particular, MMN2 was installed at the edge of a ravine, and the observed polarization is very narrow and normal to the rim for frequency greater than 2 Hz, while it becomes more isotropic at lower frequency (Figures 8 and 9). Regarding the horizontal motion amplification, MMN and MMN5 show high values of the HVSR (Figures 3 and 10) in spite of the competent local lithology. This feature could indicate that at sites MMN2 and MMN5 the peaks in the noise HVSR is an effect related mainly with the topography rather than with the underground geological structure. MMN and MMN2 are two particularly interesting sites because they are located inside the village of Mormanno, therefore understanding their site response is of interest for engineering purposes and for damage scenario forecast in case of earthquake.

At all analyzed sites the HVSR curves computed for earthquakes are much more different among them if compared with the noise HVSR curves. The small standard deviation that characterize noise results is a measure of the signal stationarity. On the other hand, earthquake signals are all different from each other, are full of body waves with their own polarization and propagation direction, therefore the difference among earthquake HVSR at each site is not surprising. At MMN9 the HVSR of the 17 analyzed earthquakes show a dispersion larger than that observed at other sites. While many events resemble very much the noise HVSR, with the

main peak around 8 Hz, some others are characterized by quite different values (Figure 6). For 11 sites out of the 15 studied, the earthquake HVSR curves are very similar to the average noise HVSR. The most evident differences between noise and earthquakes are seen at MMN, and MMN2, while minor differences are observed at MMN5 and T0713. The good agreement of noise and earthquake results for many sites is an important indication of the reliability of the HVSR method to estimate site effects through the analysis of seismic noise. The four sites where we observe differences between noise and earthquake results are all located on competent lithology, but they show horizontal polarization parallel to the slope direction. Our results indicate that much care must be taken when studying site effects. Although the results of noise analysis are very stable and reliable at all considered sites, they are not necessarily representative of site effects due to the local geological structure because there may be local conditions which prevent the efficiency of the HVSR method. In fact we found amplification and polarization of the ground motion at four sites that correlate much better with the topography than the geological structure.

The results of this work indicate that in mountainous regions where the local geology is far from a horizontally layered structure, the H/V spectral ratio alone is not sufficient to characterize the site response. More exhaustive analysis need to be performed for a satisfying interpretation of the results obtained from seismic noise. It is also interesting the fact that earthquake HVSR curves at sites with marked topographical effects do not show the same peaks, and often have lower amplitude. This result suggests an overestimation of site effects given by the noise HVSR.

Data and Resources

Seismic data used in this paper are property of Università della Calabria, and are available on

request. HVSR as a function of azimuth have been performed using the software GEOPSY (downloaded from the website *www.geopsy.org*).

Acknowledgements. The quality of this paper got considerable benefit from the comments of M. Pischiutta and an anonymous reviewer, who are both gratefully acknowledged.

Mailing address list.

Napolitano Ferdinando mail: fnapolitano@unisa.it

Anna Gervasi mail: anna.gervasi@ingv.it

Mario La Rocca mail: mario.larocca@unical.it

Ignazio Guerra mail: ignazio.guerra@unical.it

Roberto Scarpa mail: roberto.scarpa@sa.infn.it

References

Aki, K. (1993). Local site effects on weak and strong ground motion. *Tectonophysics* **218**, 93-111.

Bonamassa, O. and J. E. Vidale, (1991). Directional site resonances observed from aftershocks of the 18 October Loma Prieta earthquake, *Bull. Seism. Soc. Am.*, **81(5)**, 1945–1957.

Bonilla, L. F., H. J. Steidl, G. T. Lindley, A. G. Tumarkin, and R. Archuleta (1997). Site amplification in the San Fernando Valley, California: Variability of the site-effect estimation using the S-wave, coda, and H/V methods, *Bull. Seismol. Soc. Am*. **87**, no. 3, 710–730.

Borcherdt, R. D. (1970). Effects of local geology on ground motion near San Francisco Bay, *Bull Seism. Soc. Am.* **60**, 29-61.

Borcherdt, R. D. and J. F. Gibbs (1976). Effects of local geological conditions in the region on ground motions and intensities of the 1906 earthquakes, *Bull Seism. Soc. Am*. **66**, 467-500.

Brozzetti, F., D. Cirillo, R. de Nardis, M. Cardinali, G. Lavecchia, B. Orecchio, D. Presti, and C. Totaro (2017). Newly identified active faults in the Pollino seismic gap, southern Italy, and their seismotectonic significance, *J. Struct. Geol.,* no.**94**, 13-31, doi.org/10.1016/j.jsg.2016.10.

Buech, F., T. R. Davies, and J. R. Pettinga (2010). The little red hill seismic experimental study: topographic effects on ground motion at a bedrock-dominated mountain edifice. *Bull. Seismol.*

Soc. Am. **100 (5A)**, 2219-2229.

Cantore, L., A. Oth, S. Parolai, and D. Bindi (2011). Attenuation, source parameters and site effects in the Irpinia–Basilicata region (southern Apennines, Italy). *Journal of Seismology* **15 (2)**, 375-389.

Castro, R. R., F. Pacor, D. Bindi, G. Franceschina, and L. Luzi (2004). Site response of strong motion stations in the Umbria, central Italy, region. *Bull. Seismol. Soc. Am.* **94(2)**, 576-590.

Chávez-García, F. J., M. Rodríguez, E. H. Field, and D. Hatzfeld (1997). Topographic site effects. A comparison of two nonreference methods. *Bull. Seismol. Soc. Am.* **87(6)**, 1667-1673.

Cheloni, D., N. D'Agostino, G. Selvaggi, A. Avallone, G. Fornaro, R. Giuliani, D. Reale, E. Sansosti, and P. Tizzani (2017): Aseismic transient during the 2010-2014 seismic swarm: evidence for longer recurrence of Ml ≥6.5 earthquakes in the Pollino gap (Southern Italy)? *Scientific Reports*, DOI: 10.1038/s41598-017-00649-z

Chin, B. H., and K. Aki (1991). Simultaneous determination of source, path, and recording site effects on strong ground motion during the Loma Prieta earthquake: a preliminary result on pervasive nonlinear site effect, *Bull. Seism. Soc. Am.* **81**, 1859-1884.

Cinti, F. R., M. Moro, D. Pantosti, L. Cucci, and G. D'Addezio (2002). New constraints on the seismic history of the Castrovillari fault in the Pollino gap (Calabria, southern Italy), *J. Seismol.* **6**, 199–217.

Clemente-Chavez, A., F. R. Zúñiga, J. Lermo, A. Figueroa-Soto, C. Valdés, M. Montiel, O. Chavez, and M. Arroyo (2014). On the behavior of site effects in central Mexico (the Mexican volcanic belt). *Natural Hazards and Earth System Sciences* **14(6)**, 1391.

Cultrera, G., E. D'Alema, S. Amoroso, B. Angioni, P. Bordoni, L. Cantore, F. Cara, A. Caserta, R. Cogliano, M. D'Amico, G. Di Giulio, D. Di Naccio, D. Famiani, C. Felicetta, A. Fodarella, S. Lovati, L. Luzi, M. Massa, A. Mercuri, G. Milana, F. Pacor, M. Pischiutta, S. Pucillo, R. Puglia, G. Riccio, G. Tarabusi, M. Vassallo, and C. Mascandola (2016). Site effect studies following the 2016 Mw 6.0 Amatrice earthquake (Italy): the Emersito Task Force activities. *Ann. Geophys.* **59,** Fast Track 5, DOI: 10.4401/ag-7189.

Formisano, L. A., M. La Rocca, E. Del Pezzo, D. Galluzzo, C. Fischione, and R. Scarpa (2012). Topography effects in the polarization of earthquake signals: a comparison between surface and deep recordings. *Bollettino di Geofisica Teorica ed Applicata* **53(4)**, 471-484.

Gallipoli, M. R., M. Bianca, M. Mucciarelli, S. Parolai, and M. Picozzi (2013). Topographic versus stratigraphic amplification: mismatch between code provisions and observations during the L'Aquila (Italy, 2009) sequence. *Bull. Earthquake Eng.* **11(5)**, 1325-1336.

Gervasi, A., I. Guerra, G. Neri, B. Orecchio, D. Presti, and C. Totaro (2012): The seismic sequence in the Pollino area (2010 - …) - *31° Conv. Ann. GNGTS*, Potenza.

Gruppo di Lavoro MPS (2004). Redazione della mappa di pericolosità sismica prevista dall'Ordinanza PCM 3274 del 20 marzo 2003. Rapporto *Conclusivo per il Dipartimento della Protezione Civile, INGV,* Milano-Roma, aprile 2004, 65 pp. + 5 appendici.

Guerra, I., A. Lo Bascio, G. Luongo and A. Nazzaro, (1974): Rapporto preliminare sull'attività sismica nell'area del Comune di Mormanno (CS) - *Rapp. Tecn. Osserv. Vesuv.*

Hartzell, S. H., A. Leeds, A. Frankel, and J. Michael (1996). Site response for urban Los Angeles using aftershocks of the Northridge earthquake, *Bull. Seism. Soc. Am.* **86**, S168-S192.

Kanai, K., and T. Tanaka (1961). On microtremors, VIII, *Bull. Earthquake Res. Inst.*, Tokyo Univ, **39**, 97-115.

Kato, K., K. Aki, and M. Takemura (1995). Site amplification from coda-waves: validation and application to S-wave site response. *Bull. Seism. Soc. Am*. **85**, 467-477.

Koyanagi, S., K. Mayeda, and K. Aki (1992). Frequency-dependent site amplification factors using the S-wave coda for the island of Hawaii, *Bull. Seism. Soc. Am.* **82**, 1151-1185.

Lachet, D., C. Hatzfeld, P.-Y. Bard, N. Theodulis, C. Papaioannou, and A. Savvaidis (1996). Site effects and microzonation in the city of Thessaloniki (Greece), comparison of different approaches, *Bull. Seism. Soc. Am.* **86**, 1692-1703.

Lermo, J., and F. J. Chávez-Garcla (1993). Site effect evaluation using spectral ratios with only one station, Bull. *Seism. Soc. Am.* **83**,1574-1594.

Margheriti, L., L. Wennerberg, and J. Boatwright (1994). A comparison of coda and S-wave spectral ratio estimates of site response in the southern San Francisco Bay area., *Bull. Seism. Soc. Am.* **84**, 1815-1830.

Mayeda, K., S. Koyanagi, and K. Aki (1991). Site amplifications from S-wave coda in the Long Valley caldera region, Califonia, *Bull. Seism. Soc. Am.* **81**, 2194-2213.

Montalbetti, J. F., and E. R. Kanasewich (1970). Enhancement of Teleseismic Body Phases with a Polarization Filter, *Geophys. J. Astr.* **21**, 1970.

Nakamura, Y. (1989). A method for dynamic characteristics estimations of subsurface using microtremors on the ground surface, *Q. Rep. Railway Tech. Res. Inst. Japan* **30**, 25–33.

Nogoshi, M., and T. Igarashi (1970). On the propagation characteristics of microtremors, *Zisin* **23**, 264–280 (in Japanese with English abstract).

Nunziata, C., and M. R. Costanzo (2014). Ground motion modeling for site effects at L'Aquila and middle Aterno river valley (central Italy) for the M W 6.3, 2009 earthquake. *Soil Dynam. Earthquake Eng.* **61**, 107-123.

Panzera, F., G. Lombardo, C. Monaco, and A. Di Stefano (2015). Seismic site effects observed on sediments and basaltic lavas outcropping in a test site of Catania, Italy., *Nat. Hazards* **79(1)**, 1-27.

Panzera, F., G. Lombardo, E. Longo, H. Langer, S. Branca, R. Azzaro, V. Cicala, and F. Trimarchi (2017a). Exploratory seismic site response surveys in a complex geologic area: a case study from Mt. Etna volcano (southern Italy). *Nat. Hazards* **86(2)**, 385-399.

Panzera, F., G. Lombardo, S. Sicali, and S. D'Amico (2017b): Surface geology and morphologic effects on seismic site response: The study case of Lampedusa, Italy. *Phys. Chem. Earth, Parts A/B/C,* **98**, 62-72.

Parolai, S., S. Orunbaev, D. Bindi, A. Strollo, S. Usupaev, M. Picozzi, D. Di Giacomo, P. Augliera, E. D'Alema, C. Milkereit, and B. Moldobekov (2010). Site effects assessment in Bishkek (Kyrgyzstan) using earthquake and noise recording data. *Bull. Seismol. Soc. Am.* **100(6)**, 3068-3082.

Passarelli L., S. Hainzl, S. Sesca, F. Maccaferri, M. Mucciarelli, D. Roessler, F. Coerbi, T. Dahm, and E. Rivalta (2015). Aseismic transient driving the swarm-like seismic sequence in the Pollino range, Southern Italy. *Geophys. J. Int.* **201**,1553-1567, doi: 10.1093/gji/ggv111.

Phillips, W. S. and K. Aki (1986). Site amplification of coda waves from local earthquakes in central California., *Bull. Seism. Soc. Am.* **76**, 627-648.

Pischiutta, M., G. Cultrera, A. Caserta, L. Luzi, and A. Rovelli (2010). Topographic effects on the hill of Nocera Umbra, central Italy. *Geophys. J. Int.* **182(2)**, 977-987.

Pischiutta, M., F. Salvini, J. Fletcher, A. Rovelli, and Y. Ben-Zion (2012). Horizontal polarization of ground motion in the Hayward fault zone at Fremont, California: dominant fault-high-angle polarization and fault-induced cracks. *Geophys. J. Int.* **188(3)**, 1255-1272.

Pischiutta, M., M. Pastori, L. Improta, F. Salvini, and A. Rovelli (2014). Orthogonal relation between wavefield polarization and fast S wave direction in the Val d'Agri region: An integrating method to investigate rock anisotropy, *J Geophys Res B Solid Earth Planets* **119(1)**, 396-408.

Pischiutta, M., M. K. Savage, R. A. Holt, and F. Salvini (2015). Fracture‐related wavefield polarization and seismic anisotropy across the Greendale Fault, *J Geophys Res B Solid Earth Planets* **120(10)**, 7048-7067.

Pischiutta, M., M. Fondriest, M. Demurtas, F. Magnoni, G. Di Toro, and A. Rovelli (2017). Structural control on the directional amplification of seismic noise (Campo Imperatore, central Italy)., *Earth. Planet. Sci. Lett.* **471**, 10–18.

Pitilakis, K. (2004). Site effects. *Recent Advances in Earthquake Geotechnical Engineering an Microzonation*, pp. 139-197.

Rigano, R., F. Cara, G. Lombardo, and A. Rovelli (2008). Evidence for ground motion polarization on fault zones of Mount Etna volcano, *J. Geophys. Res. Solid Earth* **113(B10)**.

Rovida, A., R. Camassi, P. Gasperini, and M. Stucchi (2011). CPTI11, la versione 2011 del Catalogo Parametrico dei Terremoti Italiani, Milano, Bologna.

Singh, S. K., and M. Ordaz (1993). On the origin of long coda observed in the lake-bed strong-motion records of Mexico City, *Bull Seism. Soc. Am.* **83**, 1298-1306.

Steidl, J. H. (1993). Variation of site response at the UCSB dense array of portable accelerometers, *Earthquake Spectra* **9(2)**, 289-302.

Strollo, A., S. M. Richwalski, S. Parolai, M. R. Gallipoli, M. Mucciarelli, and R. Caputo. (2007). Site effects of the 2002 Molise earthquake, Italy: analysis of strong motion, ambient noise, and synthetic data from 2D modelling in San Giuliano di Puglia., *Bull. Earthquake Eng.* **5(3)**, 347.

Su, F. and K. Aki (1995). Site amplification factors in central and southern, California determined from coda waves, *Bull. Seism. Soc. Am.* **85**, 452-466.

Tertulliani, A., and L. Cucci (2014). New insights on the strongest historical earthquake in the Pollino region (southern Italy), *Seismol. Res. Lett.* **85**, 743–751, doi: 10.1785/0220130217.

Totaro, C., D. Presti, A. Billi, A. Gervasi, B. Orecchio, I. Guerra, and G. Neri (2013). The ongoing seismic sequence at the Pollino Mountains, Italy, *Seismol. Res. Lett.* **84**, no. 6, 955–962, doi: 10.1785/0220120194.

Totaro, C., L. Seeber, F. Waldhauser, M. Steckler, A. Gervasi, I. Guerra, B. Orecchio, and D. Presti (2015). An Intense Earthquake Swarm in the Southernmost Apennines: Fault Architecture from High-Resolution Hypocenters and Focal Mechanisms, *Bull. Seism. Soc. Am.* Vol. 105, No **6**, pp. 3121-3128.

Tables and figures

Table 1. Earthquakes used in this study. Distance and backazimuth are computed by using MMN as reference station.

Date, Time	Lat	Lon	Dep (km)	M	Dist (km)	Back-azimuth	MMN	MMN1	MMN2	MMN3	MMN4	MMN5	MMN6	MMN7
2010/10/06, 15:31:46	39.88	15.98	8	2.2	1	36.9			X					
2010/10/08, 02:56:43	39.88	16.00	6	2.3	1	326.3			X					
2011/11/24, 02:13:05	39.90	15.98	8	2.8	1	138.4	X				X			X
2011/10/15, 20:32:55	39.89	15.97	9	2.4	2	86.9	X	X			X			X
2010/09/25, 18:48:48	39.91	16.01	6	2.2	3	217.8			X	X				
2011/10/15, 08:38:35	39.92	15.99	6	2.0	3	179.1	X	X			X			X
2011/11/06, 11:20:35	39.92	16.02	8	2.3	4	217.7	X	X			X			X
2011/10/14, 11:44:26	39.86	15.95	8	2.4	5	45.3	X	X			X			X
2011/11/17, 08:01:52	39.94	16.02	8	2.1	6	204.6	X	X						X
2011/01/10, 10:39:00	39.91	16.07	6	1.4	7	252.6	X					X	X	
2010/12/24, 02:46:39	39.91	16.09	6	2.9	9	255.9		X			X	X	X	
2010/12/24, 03:55:20	39.85	16.08	5	1.9	9	300.8		X				X	X	
2010/12/24, 05:08:09	39.87	16.09	5	1.6	9	285.3		X			X	X	X	
2011/04/10, 02:48:24	39.81	16.00	7	2.3	9	354.9		X					X	X
2011/01/20, 16:00:05	39.81	16.06	10	1.2	10	326.6		X			X	X		
2010/10/03, 13:45:24	39.94	15.87	9	2.0	12	117.9		X	X					
2011/08/12, 16:33:11	39.91	15.85	8	2.1	12	100.0	X	X			X			X
2010/12/25, 07:22:06	39.79	16.07	6	1.7	13	328.8	X				X	X		
2011/07/22, 17:44:24	39.83	15.86	39	2.2	13	58.7		X			X		X	X
2011/02/23, 22:26:12	39.80	16.10	10	2.0	14	317.2		X		X	X		X	
2011/10/12, 18:19:03	39.90	16.16	7	2.1	14	266.0	X	X			X			X
2011/01/07, 18:19:46	39.91	16.18	6	2.4	17	262.5	X			X	X	X	X	
2010/11/09, 08:43:19	40.05	15.93	6	3.6	18	163.7	X	X	X	X				
2010/09/22, 21:04:49	39.92	16.21	8	2.5	19	260.2				X				
2011/01/05, 16:21:22	39.82	15.53	273	2.5	40	78.5	X				X	X	X	
2011/05/19, 14:50:51	39.06	15.13	298	4.6	118	38.3							X	
2010/10/15, 05:21:19	38.87	16.63	37	4.3	126	334.4		X	X	X	X			
2010/11/03, 18:13:02	39.98	13.27	506	5.4	232	91.6		X	X		X			
2010/11/03, 00:56:54	43.74	20.69	2	5.3	578	223.9		X	X	X	X			

Table 2. Earthquakes used in this study (continuation).

Date, Time	Lat	Lon	Dep (km)	M	Dist (km)	Back-azimuth	MMN	MMN1	MMN4	MMN6	MMN9	MMNA	MMNB	T0711	T0713	T0714	T0716
2011/12/13, 11:08:17	39.89	16.02	8	2.1	3	272.1	X	X	X					X	X	X	
2011/12/27, 01:18:12	39.89	16.03	9	2.5	3	271.5		X						X	X	X	
2011/11/28, 12:25:03	39.92	16.03	8	1.5	4	226.0	X							X			
2011/12/02, 09:31:10	39.92	16.01	9	2.7	4	207.0	X	X						X	X		
2012/02/21, 12:24:47	39.93	16.00	9	2.9	4	190.4	X	X							X	X	
2012/04/24, 04:06:08	39.90	16.04	7	2.0	4	256.4	X										X
2011/12/01, 18:02:47	39.93	16.01	9	2.5	5	200.8	X	X	X					X	X		
2011/12/07, 12:58:19	39.92	16.01	8	2.3	5	207.0		X						X	X	X	
2012/01/20, 21:46:31	39.90	16.04	7	2.2	5	256.4	X	X			X			X	X	X	
2012/01/24, 12:16:18	39.9	16.0	8	2.0	5	226.0	X	X			X			X	X	X	

Date, Time	Lat	Lon	Dep (km)	M	Dist (km)	Back-azimuth	MMN	MMN1	MMN4	MMN6	MMN9	MMN A	MMN B	T0711	T0713	T0714	T0716
	2	3															
2011/12/08, 10:06:43	39.94	16.01	9	2.3	6	196.8								X		X	
2011/12/10, 14:53:25	39.94	16.00	6	2.6	6	188.3								X	X	X	
2016/08/06, 11:29:34	39.91	16.06	9	2.5	6	250.2	X	X					X				
2012/05/17, 10:44:50	39.89	16.10	8	2.2	9	270.6	X				X						X
2012/05/16, 01:36:11	39.89	16.11	8	2.3	10	270.5	X	X			X						X
2012/05/28, 01:06:26	39.87	16.10	8	4.3	10	283.9		X	X	X					X		X
2012/05/28, 01:32:10	39.91	16.10	7	3.2	10	257.1		X	X	X					X		X
2012/05/28, 22:50:53	39.90	16.10	8	2.9	10	263.8	X	X	X	X	X						X
2012/05/29, 04:04:35	39.89	16.11	8	2.9	10	270.5	X	X									
2012/06/05, 21:46:54	39.89	16.10	9	2.7	10	270.6	X	X							X		
2013/06/25, 19:56:00	39.91	16.11	8	2.7	10	258.2	X	X		X	X						
2013/07/02, 04:21:55	39.90	16.11	7	2.3	10	264.3	X	X		X	X						
2012/05/28, 05:01:04	39.88	16.11	8	2.2	11	276.7		X									X
2012/05/30, 16:17:24	39.87	16.12	8	2.8	11	281.8	X										X
2016/10/29, 11:58:04	39.95	15.83	275	4.1	15	115.6	X	X					X				
2012/03/10, 09:54:46	39.90	16.18	9	2.2	16	266.4	X	X			X			X	X	X	
2012/02/13, 19:35:53	39.88	16.19	8	2.0	17	274.1	X	X						X	X	X	
2014/10/17, 16:40:23	39.91	15.72	284	3.4	23	95.1	X					X					
2012/04/01, 19:21:25	39.72	15.77	286	3.9	27	44.7	X			X	X				X	X	
2012/10/16, 15:10:57	39.67	15.74	276	4.6	33	41.0	X	X		X	X						
2012/05/31, 03:16:21	39.87	15.57	8	3.0	36	86.2		X	X	X	X						X
2011/12/14, 17:59:49	39.37	16.18	6	3.1	60	344.4		X	X	X				X	X	X	
2011/12/17, 23:20:15	39.37	16.16	8	3.4	60	345.9		X	X	X				X	X	X	
2012/07/04, 13:27:13	38.42	15.16	175	4.1	88	53.4					X						
2014/08/04, 05:54:00	38.69	15.73	175	4.3	135	9.4						X					
2012/09/27, 01:08:22	41.18	14.92	10	4.2	170	147.3	X	X		X							
2012/11/13, 07:06:33	38.23	15.85	78	4.4	185	3.7	X			X							
2012/08/28, 23:13:15	38.20	15.73	49	4.5	190	6.7		X			X						
2014/10/09, 22:58:00	38.47	14.71	25	4.3	192	34.5	X			X		X					
2016/10/28, 20:02:43	39.26	13.54	481	5.8	221	70.7	X	X			X		X				
2014/11/10, 20:48:15	39.24	19.47	5	4.1	307	284.7	X			X		X					

Date, Time	Lat	Lon	Dep (km)	M	Dist (km)	Back-azimuth	MMN	MMN1	MMN4	MMN6	MMN9	MMNA	MMNB	T0711	T0713	T0714	T0716
2016/10/15, 20:14:49	39.77	20.64	20	5.2	397	273.4	X	X			X		X				
2016/10/30, 06:40:17	42.83	13.11	9	6.5	405	142.7	X	X			X		X				
2016/10/26, 19:18:05	42.90	13.12	8	5.9	411	143.4	X				X		X				
2014/02/03, 03:08:46	38.29	20.31	10	6.1	413	291.1	X										
2016/11/01, 07:56:40	42.99	13.13	8	4.8	419	144.3	X	X			X		X				
2014/01/26, 18:45:07	38.20	20.36	10	5.1	420	297.8	X										
2014/11/07, 07:41:40	38.15	20.43	20	5.1	429	298.1				X		X					
2014/01/26, 13:55:44	38.23	20.48	10	5.9	430	296.8	X										
2014/11/08, 23:15:43	38.10	20.40	10	5.1	430	298.9	X					X					
2014/10/24, 23:43:16	38.91	21.09	12	5.0	451	285.5	X					X					
2014/11/07, 17:13:02	38.32	22.25	10	5.0	567	289.8						X					
2016/07/30, 17:26:24	35.30	22.90	35	5.1	794	312.0	X	X					X				
2016/09/23, 23:11:20	45.76	26.63	94	5.6	1084	236.7	X				X		X				

Table 3. Relationship between polarization and slope

Site	Angle between polarization and slope	Site	Angle between polarization and slope
MMN	Parallel	MMN1	Roughly normal
MMN2	Parallel	MMN3	Roughly normal
MMN4	Parallel	MMN6	Roughly normal
MMN9	Parallel		
MMNB	Parallel	MMN5	Oblique, roughly normal
T0711	Parallel, normal to the ridge		
T0716	Parallel, normal to the ridge	MMNA	Undefined (isotropic)
T0713	Roughly parallel	T0714	Undefined (isotropic)
MMN7	Roughly parallel		

Table 4. Relationship between polarization and known faults

Site	Distance to the fault	Angle between polarization and strike
MMN4	About 200 m	60 – 70
MMN9	170 m	60 – 70
MMNB	30 m	40 – 50
T0711	240 m	85 – 90

T0713	30 m	35 – 40

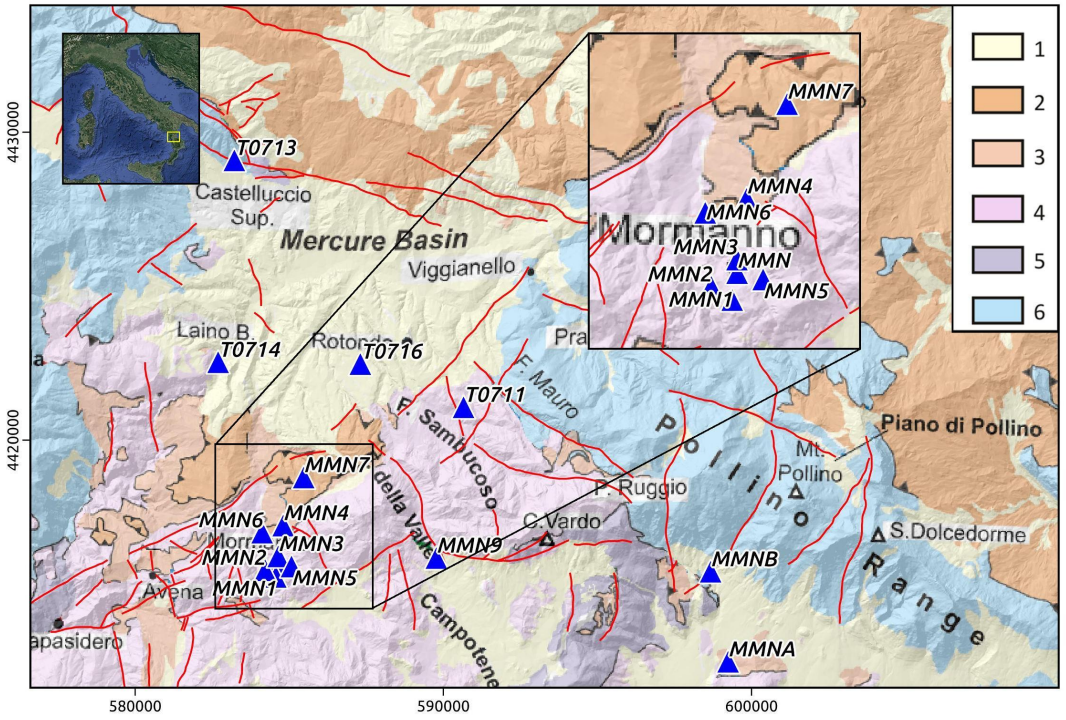

Figure 1. Geological and topographic map of the western Mt. Pollino area modified after Brozzetti et al. (2017). Red lines show known faults, while blue triangles represent seismic stations used in this study. Key: 1 = Sin-extensional deposits of the continental basins (Mercure, Campotenese and Morano Calabro basins) and of the marine, evolving to continental, Castrovillari basin (Pleistocene-Holocene); 2 = Allochthonous Liguride unit (mainly Late Cretaceous); 3 = Fiume Lao schist formation (Burdigalian); 4 = Apennine Platform western Unit (Verbicaro Unit, Late Triassic-Early Miocene); 5 = Metalimestones and metapelites of the San Donato metamorphic core (Middle-Late Triassic?); 6 = Apennine Platform eastern Unit (Pollino Unit, Late Triassic-Late Cretaceous).

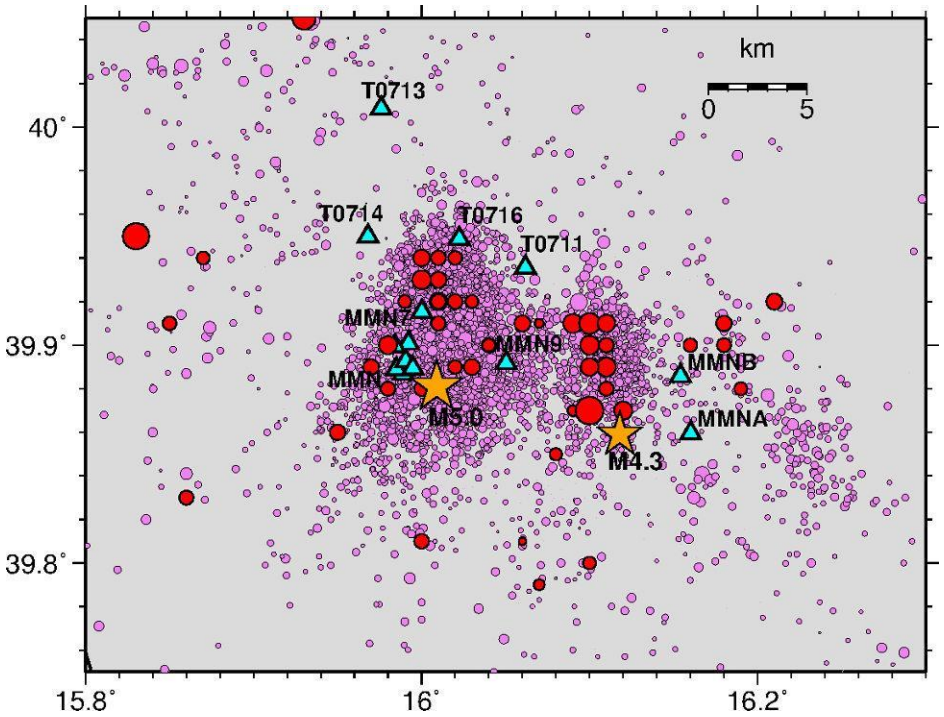

Figure 2. Epicenters of the earthquakes located in the area of Mt. Pollino from 2010 to 2014. The symbol size is proportional to magnitude. Red circles show the local earthquakes analyzed in this work (Table 1 and Table 2), while the two mainshocks are shown by orange stars. Seismic stations used in our analysis are shown by cyan triangles.

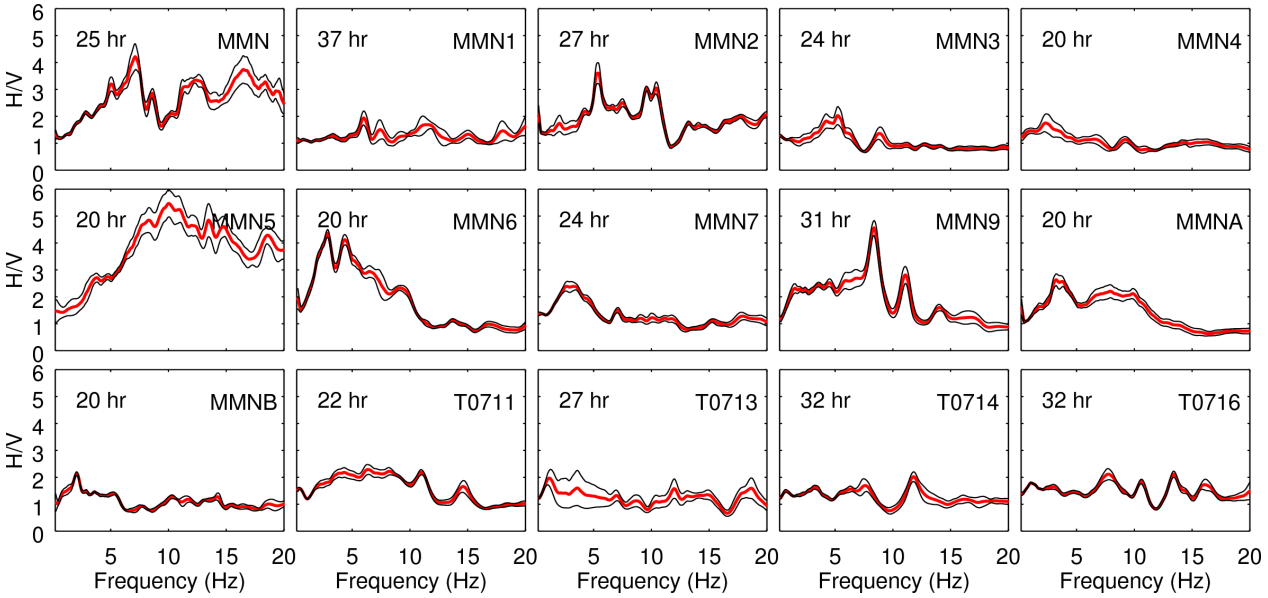

Figure 3. HVSR average curve and its standard deviation obtained from the analysis of noise recordings at the 15 studied sites. The number of hours of analyzed data is written in each plot.

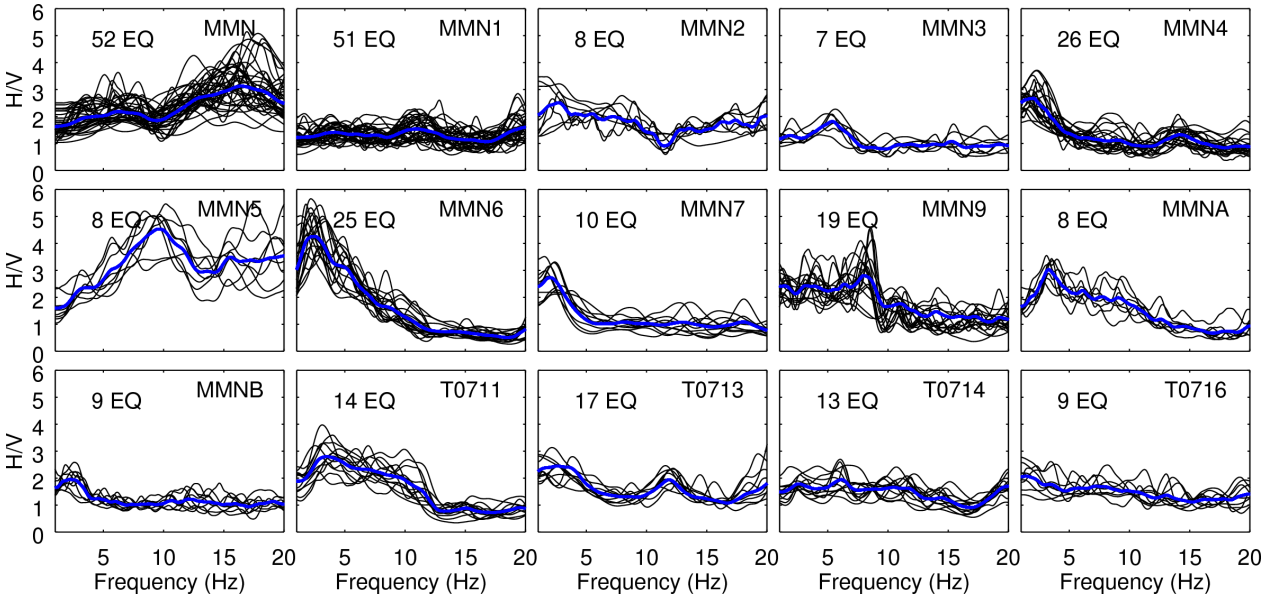

Figure 4. Results of HVSR obtained from the analysis of earthquakes at the studied 15 sites. Each plot shows the results of individual events by black line and the average by blue line. The number of analyzed earthquakes is written in each plot.

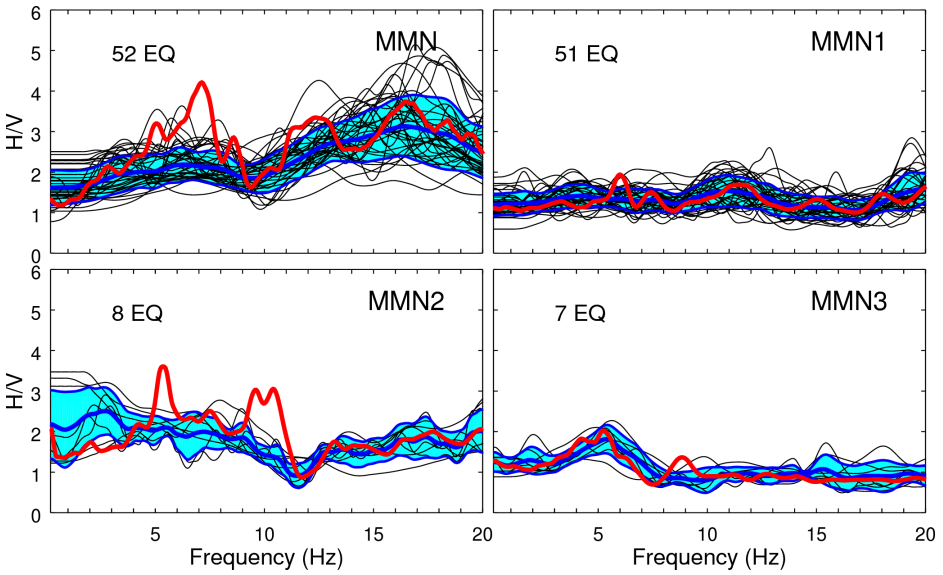

Figure 5. Comparison between earthquakes (black) and average seismic noise (red) HVSR for four of the analyzed sites: MMN, MMN1, MMN2, MMN3. The blue lines and cyan color show the average of earthquake HVSR and its standard deviation.

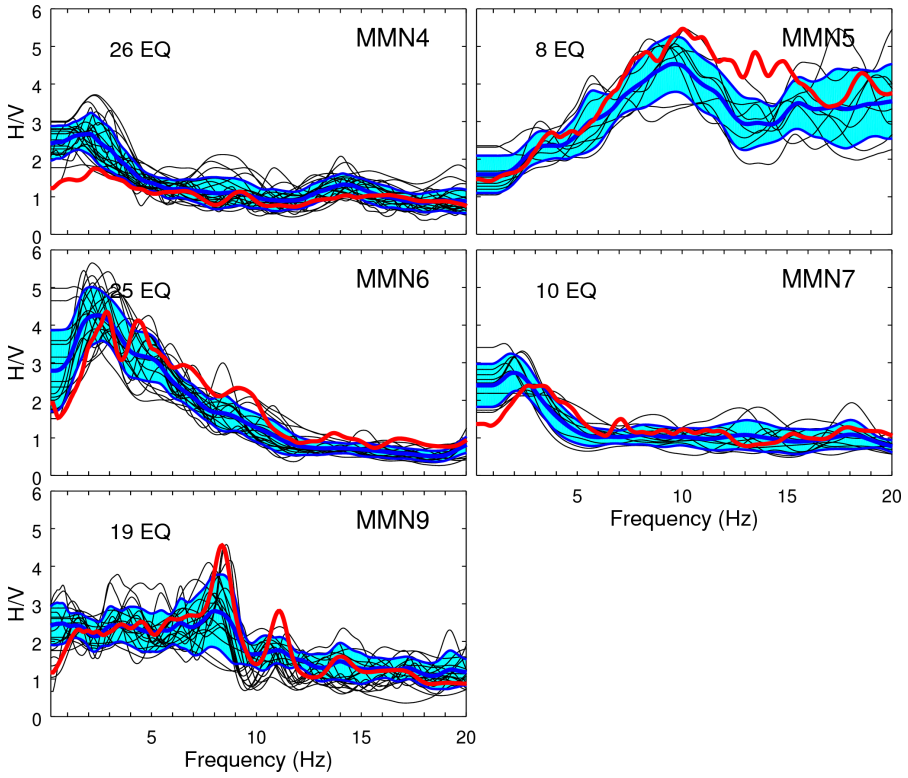

Figure 6. Comparison between earthquakes (black) and average seismic noise (red) HVSR for five of the analyzed sites: MMN4, MMN5, MMN6, MMN7, MMN9. The blue lines and cyan color show the average of earthquake HVSR and its standard deviation.

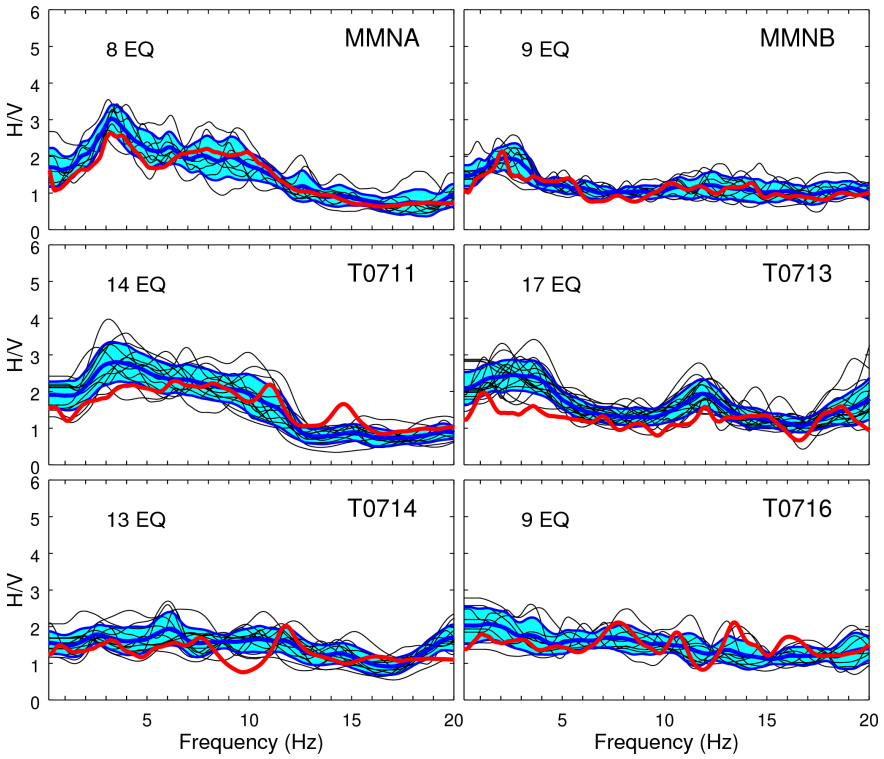

Figure 7. Comparison between earthquakes (black) and average seismic noise (red) HVSR for six of the analyzed sites: MMNA, MMNB, T0711, T0713, T0714, T0716. The blue lines and cyan color show the average of earthquake HVSR and its standard deviation.

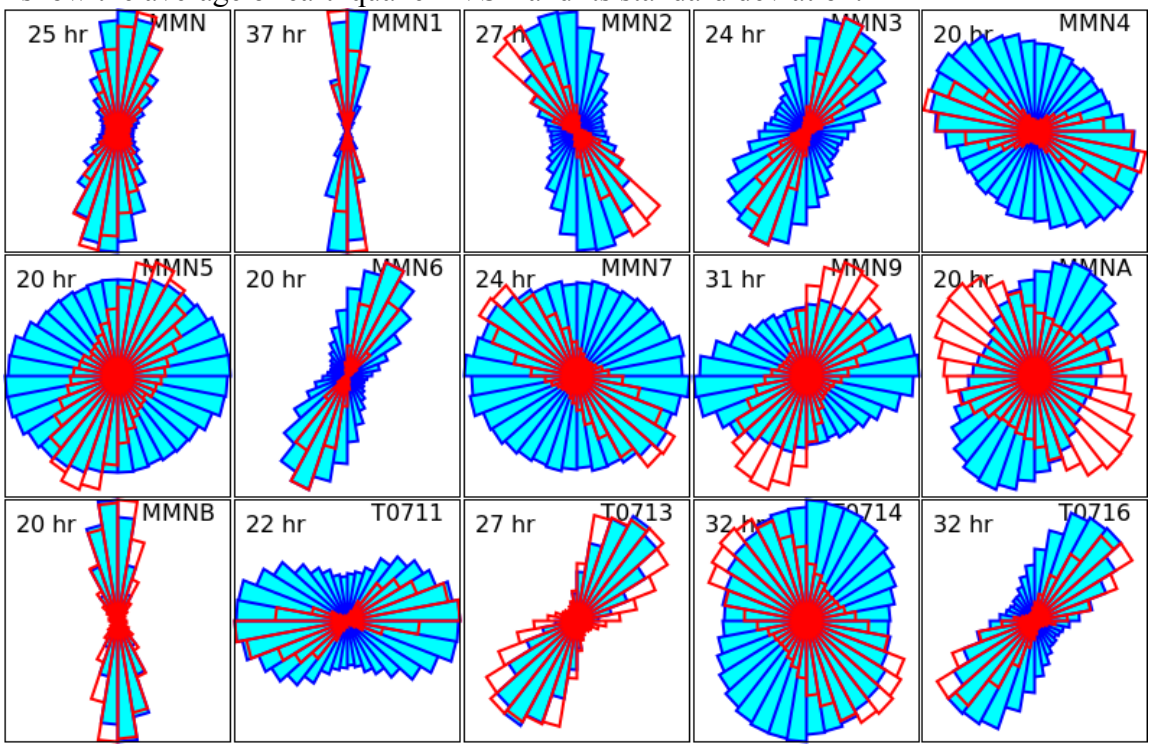

Figure 8. Stacked and normalized polar histograms showing the distributions of polarization azimuth in the frequency band 1 – 2 Hz (blue) and 2 - 4 Hz (red) at each station. The number of hours of analyzed seismic noise is written in each plot.

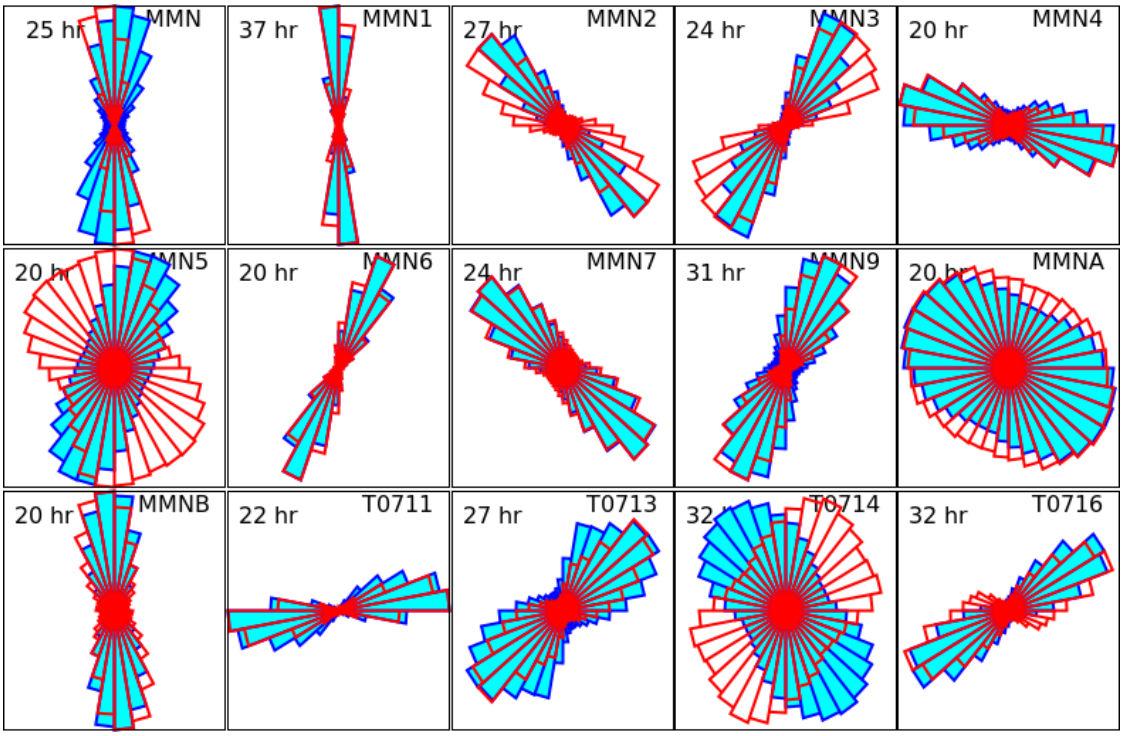

Figure 9. Stacked and normalized polar histograms showing the distributions of polarization azimuth in the frequency band 3 - 5 Hz (blue) and 4 – 8 Hz (red) at each station. The number of hours of analyzed seismic noise is written in each plot.

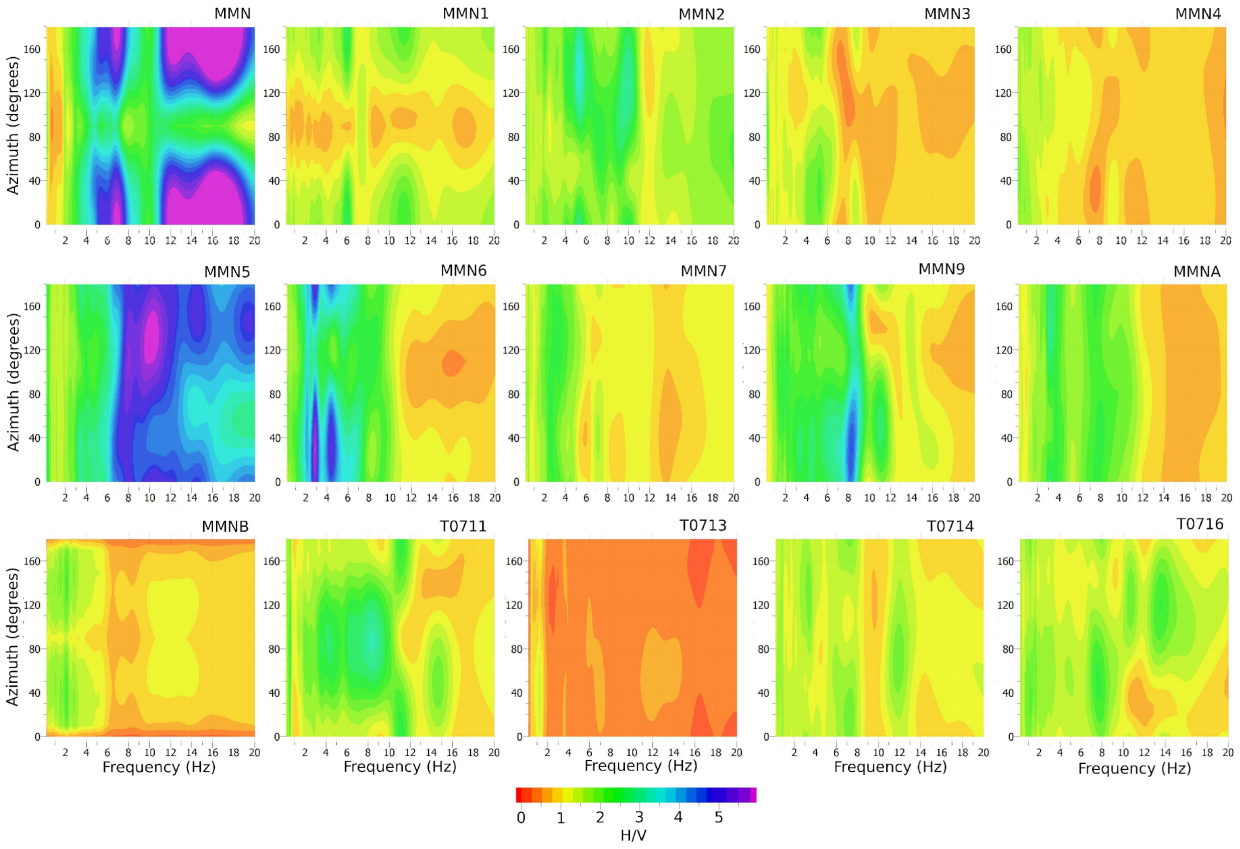

Figure 10. Frequency – azimuth H/V analysis. Each plot shows the H/V ratio versus frequency and azimuth. The colors scale shown at the bottom is the same for all plots.